Model of laser cooling in the Yb^{3+}-doped fluorozirconate glass ZBLAN

Markus P. Hehlen and Richard I. Epstein
Los Alamos National Laboratory, Los Alamos, New Mexico 87545, USA

Hiroyuki Inoue
Institute of Industrial Science, The University of Tokyo, Tokyo 153-8505, Japan

(Received 19 June 2006; revised manuscript received 15 December 2006; published 12 April 2007)

A quantitative description of optical refrigeration in Yb^{3+}-doped ZBLAN glass in the presence of transition-metal and OH impurities is presented. The model includes the competition of radiative processes with energy migration, energy transfer to transition-metal ions, and multiphonon relaxation. Molecular dynamics calculations of pure ZBLAN and ZBLAN doped with transition-metal ions provide the structural information that, when combined with spectroscopic data, allows for the calculation of electric-dipole energy-transfer rates in the framework of the Dexter theory. The structural data is further used to extend the traditional energy-gap law to multiphonon relaxation via vibrational impurities. The cooling efficiency is sensitive to the presence of both 3*d* metal ions with absorption in the near infrared and high-frequency vibrational impurities such as OH. The calculation establishes maximum impurity concentrations for different operating temperatures and finds Cu^{2+}, Fe^{2+}, Co^{2+}, Ni^{2+}, and OH to be the most problematic species. Cu^{2+} in particular has to be reduced to <2 ppb, and Fe^{2+}, Co^{2+}, Ni^{2+}, and OH have to be reduced to 10–100 ppb for a practical ZBLAN:Yb^{3+} optical cryocooler to operate at 100–150 K.

DOI: 10.1103/PhysRevB.75.144302 PACS number(s): 33.80.Ps, 78.20.Bh, 78.55.Qr

I. INTRODUCTION

Optical refrigeration of a solid was first experimentally demonstrated in 1995 with the ytterbium-doped fluorozirconate glass ZBLANP:Yb^{3+}.[1] Laser-induced cooling has since been observed in a range of glasses and crystals doped with Yb^{3+} [ZBLANP,[2–7] ZBLAN,[8,9] CNBZn,[10,11] BIG,[10,11] $KGd(WO_4)_2$,[12] $KY(WO_4)_2$,[13] YAG,[14] Y_2SiO_5,[14] KPb_2Cl_5,[11,15] BaY_2F_8 (Refs. 16 and 17)], doped with Tm^{3+} [ZBLANP,[18–20] BaY_2F_8 (Ref. 21)], and doped with Er^{3+} [CNBZn (Ref. 22), KPb_2Cl_5 (Ref. 22)]. The mechanism of anti-Stokes fluorescent cooling has the potential to reach cryogenic temperatures and to enable solid-state refrigerators that can provide highly reliable, noise-free, and vibration-free cooling of sensitive electronic or optoelectronic components such as low-noise amplifiers and IR cameras in space-based systems.

The most thoroughly studied rare-earth-doped solid for optical refrigeration is ZBLAN:Yb^{3+}, a fluorozirconate glass with a representative composition of 53%ZrF_4-20%BaF_2-4%LaF_3-3%AlF_3-20%NaF (mol. %) and typically doped with 1–2% Yb^{3+} (Yb^{3+} replacing La^{3+}). There also exists a large body of literature on efforts to use ZBLAN glass for long-haul fiber-optic applications.[23,24] The developments during the past decade have resulted in device-level cooling with ZBLAN:Yb^{3+} to the record-low temperature of 208 K in our laboratory.[7] However, to enable practical optical cryocoolers that can favorably compete with established thermoelectric cooling technologies, base temperatures in the range of 100–150 K are needed. ZBLAN:Yb^{3+} has the potential to cool to 100–150 K with efficiencies of around 1–3 % (see Sec. III). The corresponding heat lift of a few hundred milli-Watts when pumped by a ~10 Watt laser would enable a wide range of cooling applications. The main limitation towards realizing this desired performance has been the substantial variation in the cooling performance found for nominally identical commercial ZBLAN:Yb^{3+} samples. The cooling efficiency is very sensitive to "parasitic" heating by impurities[25] and, with commercial ZBLAN:Yb^{3+} not currently optimized for this application, it is not surprising to find unacceptably large lot-to-lot cooling performance variations. These substantial variations in the cooling material itself have made it difficult to engineer and optimize the other components of an integrated cryocooler device in a systematic fashion. To advance optical refrigeration towards practical devices it is therefore necessary to develop a detailed understanding of the various factors affecting the intrinsic cooling efficiency of the material and to address them by material preparation techniques tailored to the requirements of this application.

This study presents a quantitative model of optical refrigeration in ZBLAN:Yb^{3+} in the presence of transition-metal and OH impurities. Our goal is to determine upper concentration limits for specific impurities in this material. Rare-earth ions such as Er^{3+}, Tm^{3+}, Ho^{3+}, Dy^{3+}, Sm^{3+}, and Pr^{3+} can also cause parasitic heating by nonradiative relaxation following energy transfer from Yb^{3+}. The most likely rare earths associated with Yb^{3+} as impurities are Er^{3+} and Tm^{3+}. Goldner *et al.*[26] have found that the degradation of the ZBLAN:Yb^{3+} cooling efficiency by Er^{3+} and Tm^{3+} is negligible if their concentrations are below ~5 and ~500 ppm, respectively. We will show that the impact of transition-metal and OH impurities on the cooling efficiency is much more severe, and we will therefore exclude rare-earth impurities from our analysis.

Section II gives a short review of laser cooling with rare-earth ions and points out today's limitations in creating practical optical refrigerators. Section III presents a model of laser cooling in ZBLAN:Yb^{3+} that takes into account radiative processes (Sec. III A) and competing nonradiative processes (Sec. III B). Molecular dynamics calculations of

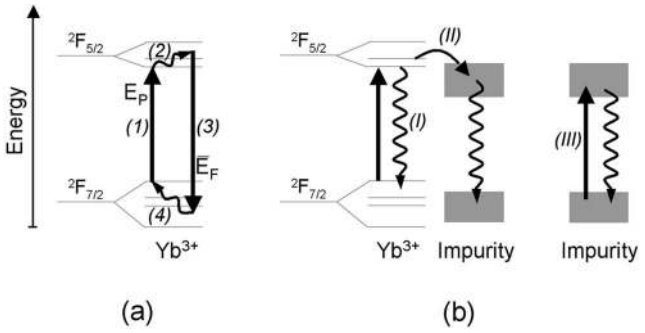

FIG. 1. (a) Ideal case of optical refrigeration using radiative transitions between the two crystal-field-split multiplets of Yb^{3+} in a solid. E_P and $\bar{E}_F$ are the pump energy and mean fluorescence energy, respectively. The ideal cooling cycle consists of (1) absorption, (2) excited-state thermalization, (3) Anti-Stokes fluorescence, and (4) ground-state thermalization. (b) The most important processes competing with the Yb^{3+} ideal cooling cycle and introducing parasitic heating via multiphonon relaxation (wiggly arrows): (I) multiphonon relaxation of the $^2F_{5/2}$ excited state, (II) energy transfer from the $^2F_{5/2}$ excited state to an impurity followed by multiphonon relaxation, and (III) background absorption by an impurity followed by multiphonon relaxation.

ZBLAN form the basis for deriving spatial ion distributions and calculating corresponding electric-dipole radial integrals (Sec. III C). This structural data is then used in conjunction with available spectroscopic data to calculate energy-transfer rates (Sec. III D) and multiphonon relaxation rates (Sec. III E). We use this model in Sec. IV to calculate upper impurity concentration limits in ZBLAN:1 % Yb^{3+} for different target operating temperatures.

II. LASER COOLING WITH RARE-EARTH IONS

Optical refrigeration is a mechanism for cooling certain solids with laser light. The cooling is a result of anti-Stokes fluorescence, a process in which the solid absorbs light at one frequency and reemits light at a higher frequency. The accompanying difference in photon energies is supplied by thermal vibrations of the solid. This extraction of thermal energy by photons tends to cool the solid. Anti-Stokes fluorescence cooling can be realized with rare-earth ions such as Yb^{3+} by using radiative transitions between two $4f$ multiplets that are each split by crystal-field interactions [Fig. 1(a)]. For Yb^{3+}, the cooling cycle consists of (1) absorption of a pump photon from the $^2F_{7/2}$ ground-state multiplet in thermal equilibrium, (2) thermalization of the $^2F_{5/2}$ excited-state multiplet, (3) reemission of a photon from the $^2F_{5/2}$ excited-state multiplet in thermal equilibrium, and (4) thermalization of the $^2F_{7/2}$ ground-state multiplet. If the pump photon energy, E_P, is smaller than the mean energy of the emitted photons, $\bar{E}_F$, then the sum of the thermalization steps will be endothermic and cause a net flow of energy from the vibrational subsystem to the electronic subsystem of the solid, producing a cooling effect. In the absence of any other processes, the cooling efficiency in this ideal case is given by

$$\eta_{cool} = \frac{\bar{E}_F - E_P}{E_P} = \frac{\lambda_P - \bar{\lambda}_F}{\bar{\lambda}_F}, \tag{1}$$

where $\bar{E}_F - E_P$ is on the order of at most a few kT. The smaller the energy gap between the two multiplets, i.e., the smaller E_P relative to kT, the higher the cooling efficiency. Even at this atomistic level there exist, however, competing processes that tend to introduce parasitic heating and thus lower the cooling efficiency. The most important competing processes in the case of Yb^{3+}, illustrated in Fig. 1(b), are (I) multiphonon relaxation of the $^2F_{5/2}$ excited state via interactions with impurities having high-energy vibrational modes, (II) nonradiative energy transfer from the $^2F_{5/2}$ excited state to an nearby impurity followed by multiphonon relaxation, and (III) background absorption by an impurity followed by multiphonon relaxation. Maximizing the cooling efficiency therefore requires minimizing impurity concentrations.

III. MODEL OF LASER COOLING IN ZBLAN:Yb^{3+}

A. Radiative transitions

The maximum laser-cooling performance of a rare-earth doped solid is determined by the absorption and fluorescence spectra of the electronic transitions used for the cooling cycle. The Yb^{3+} fluorescence spectrum, and thus the mean fluorescence wavelength $\bar{\lambda}_F(T)$, is solely determined by the nature of the host material and by the temperature, T. In contrast, the pump wavelength, λ_P, can be chosen freely—in principle—as long as $\lambda_P > \bar{\lambda}_F$ to achieve $\eta_{cool} > 0$ [Eq. (1)]. As λ_P is increased however, the corresponding absorption coefficient, $\alpha(\lambda_P, T)$, drops exponentially in the long-wavelength tail of the absorption spectrum (see Fig. 2), and the respective absorption length increases dramatically. An optical cryocooler device will incorporate mirrors to create a cavity that confines the pump light, but there are practical limitations to the achievable trapping length: the mirror reflectivities will be less than unity, and some of the pump light will escape through the pump input aperture. For example, with pump-light confinement inside a 1 cm^3 sample having two parallel mirrored surfaces with a reflectivity of 99.9% and a 600 μm diameter aperture in one of the mirrors, one achieves (neglecting coherence effects) a $(1/e)$ trapping length of $\sim$400 cm. This in turn requires $\alpha(\lambda_P, T) > 2.5 \times 10^{-3}$ cm^{-1} for absorption to be competitive with cavity losses and thereby sets an upper limit on λ_P at a given temperature T. In the following calculations we choose λ_P such that $\alpha(\lambda_P, T) = 5 \times 10^{-3}$ cm^{-1}, a value that is considered representative of first-generation devices. Future improvements in the dielectric mirrors and the pump-light coupling will enable the use of a lower $\alpha(\lambda_P, T)$, i.e., a higher λ_P, and therefore achieve higher cooling efficiencies. Figure 2 shows absorption and fluorescence spectra of ZBLAN:Yb^{3+} at several temperatures. The $\bar{\lambda}_F(T)$ and $\lambda_P(T)$ derived from these

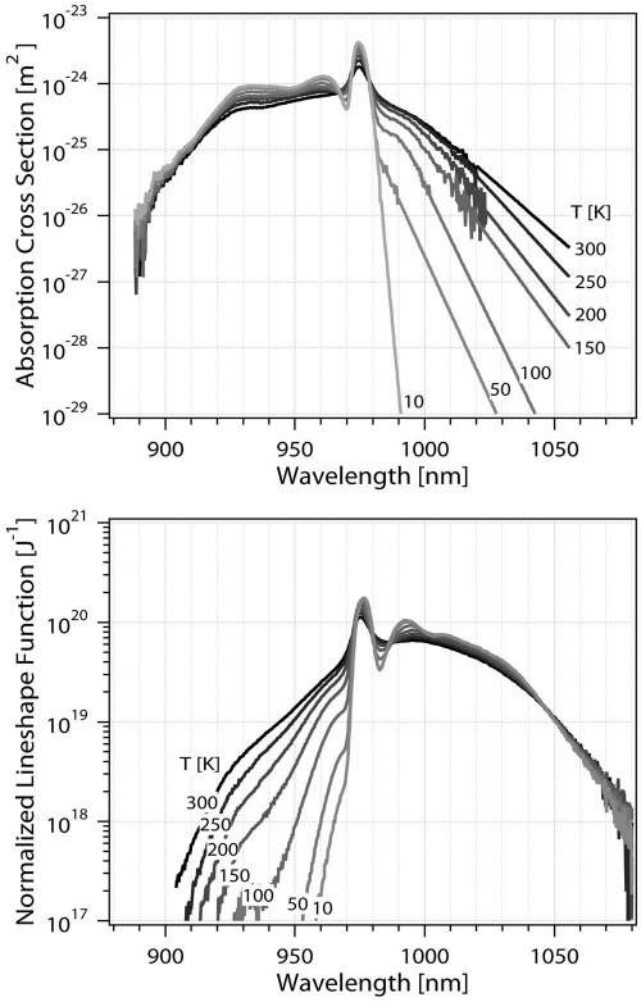

FIG. 2. Spectral data for ZBLAN: Yb^{3+} adapted from Ref. 27. Top: Absorption cross section of Yb^{3+} in ZBLAN as a function of temperature, shown with exponential long-wavelength extrapolations. Bottom: Normalized line shape function of the Yb^{3+} fluorescence in ZBLAN as a function of temperature.

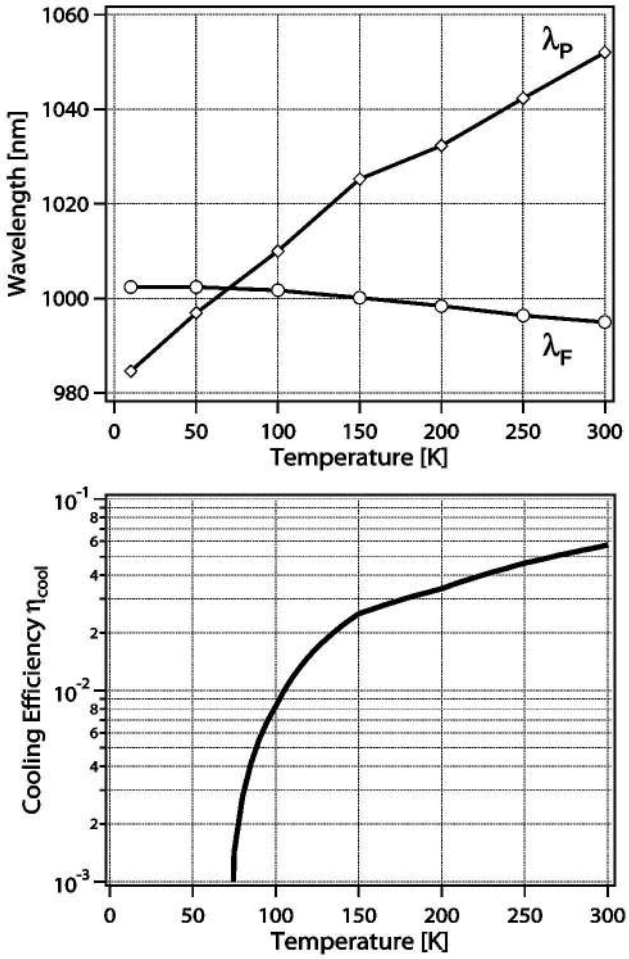

FIG. 3. Top: Mean fluorescence wavelength $\bar{\lambda}_F$ (circles) and pump wavelength λ_P for $\alpha(\lambda_P,T)=5\times10^{-3}$ cm^{-1} (diamonds) in ZBLAN: 1% Yb^{3+} derived from the spectra shown in Fig. 2. Bottom: Ideal cooling efficiency calculated from $\bar{\lambda}_F(T)$ and $\lambda_P(T)$ using Eq. (1). Optical refrigeration is possible if $\lambda_P(T)>\bar{\lambda}_F(T)$, that is for temperatures above ~70 K.

spectra are shown in Fig. 3 along with the calculated "ideal" cooling efficiency [Eq. (1)] in this material. Cooling efficiencies of 1–3 % are possible in the 100–150 K temperature range, and a practical lower temperature limit is reached at ~70 K, in agreement with previous work.[28,29]

B. Competing processes

In contrast to other rare-earth ions, Yb^{3+} is unique in that its $[Xe]4f^{13}$ electron configuration produces only a ^2F manifold that is split into a $^2F_{7/2}$ ground-state and a $^2F_{5/2}$ excited-state multiplet by spin-orbit coupling, with the $^2F_{5/2}$-$^2F_{7/2}$ energy difference of ~10 000 cm^{-1} corresponding to optical transitions at wavelengths around 1 μm. In a solid, the $^2F_{7/2}$ and $^2F_{5/2}$ multiplets are further split by crystal-field interactions into 4 and 3 Kramers doublets, respectively, as schematically shown in Fig. 1(a). The absence of any other $4f$ electronic states in Yb^{3+} greatly simplifies the excitation dynamics compared to other rare-earth ions and, specifically, excludes energy-transfer upconversion and excited-state absorption that can be present in other rare-earth-doped solids.[26] The three competing processes shown in Fig. 1(b) however may all be present and affect the cooling efficiency of an Yb^{3+}-based optical refrigerator.

Yb^{3+} is sensitive to parasitic heating: If the $^2F_{5/2}$ excited state relaxes nonradiatively rather than radiatively, an energy of ~10 000 cm^{-1} is released as heat into the solid, and a great number of successful cooling cycles, each extracting only a few kT of heat, are required to compensate for this one heating event. Assuming that all multiphonon relaxation events release the entire excitation energy, E_P, as heat into the solid, we can describe the competition of relaxation processes with the flow chart shown in Fig. 4. The competition between heating and cooling events, and therefore the cooling efficiency, is then determined by three probabilities. p_a is the probability of absorption by Yb^{3+}, i.e., the competition between the Yb^{3+} and the impurity absorption coefficients at the pump wavelength λ_p. p_a is defined as

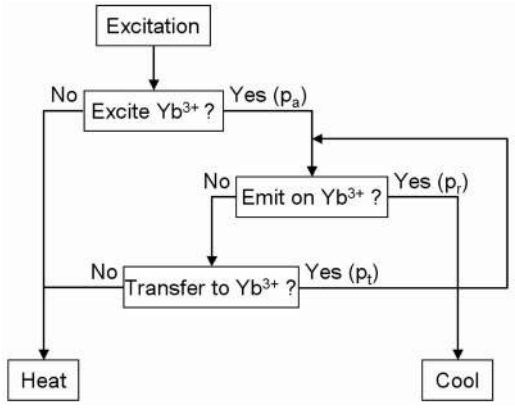

FIG. 4. Flow chart of relaxation processes in an Yb^{3+}-based optical refrigerator material. The cooling efficiency is determined by the three probabilities describing the competition between heating and cooling events: p_a is the probability that the excitation is created on Yb^{3+} rather than on an impurity, p_r is the probability that an excited Yb^{3+} decays radiatively rather than undergoing a nonradiative process, and p_t is the probability that an excited Yb^{3+} transfers its excitation nonradiatively to a neighboring Yb^{3+} rather than to an impurity.

$$p_a(\lambda_p,T)=\frac{\alpha_0(\lambda_p,T)}{\sum_{i=0}^{N}\alpha_i(\lambda_p,T)}, \tag{2}$$

where $\alpha_0(\lambda_p,T)$ is the Yb^{3+} absorption coefficient and $\alpha_{i>0}(\lambda_p,T)$ are the absorption coefficients of the N types of impurities at the pump wavelength λ_p. Conversely, the quantity $(1-p_a)$ is the probability of background absorption [process "III" in Fig. 1(b)]. The second competition, defining the *intrinsic* Yb^{3+} (single ion) quantum efficiency, is the probability p_r that an excited Yb^{3+} relaxes radiatively (r) rather than nonradiatively (nr), and it is defined as

$$p_r(T)=\frac{w_0^{(r)}(T)}{w_0^{(r)}(T)+\sum_{i=0}^{N}w_{0i}^{(nr)}(T)}, \tag{3}$$

where $w_0^{(r)}(T)$ is the Yb^{3+} radiative relaxation rate and $w_{0i}^{(nr)}(T)$ is the rate of nonradiative energy transfer from an excited Yb^{3+} either to another Yb^{3+} ($i=0$) or to any of the N types of impurities ($i>0$). The impurities can be (1) metal ions other than Yb^{3+} such as transition metal ions [Eq. (10), Sec. III D] and (2) vibrational impurities such as OH [Eq. (14), Sec. III E]. We assume that impurities are nonradiative "traps," i.e., once excited they rapidly decay by multiphonon relaxation. We therefore neglect energy "backtransfer" from the impurities to Yb^{3+}. The third competition is between $Yb^{3+}\rightarrow Yb^{3+}$ nonradiative energy migration and nonradiative energy transfer from Yb^{3+} to any of the N types of impurities. The respective probability p_t is defined as

$$p_t(T)=\frac{w_{00}^{(nr)}(T)}{\sum_{i=0}^{N}w_{0i}^{(nr)}(T)}. \tag{4}$$

Note that $Yb^{3+}\rightarrow Yb^{3+}$ nonradiative energy migration *per se* is unproblematic since, within the framework of this description, it is assumed resonant and therefore neither deposits heat into nor extracts heat from the solid (see Sec. III D). Note that this model neglects radiative energy transfer, which depends on device-specific factors such as sample geometry, mirror reflections, and bulk scattering.

The probability for a relaxation to result in a cooling event, i.e. the *net* Yb^{3+} quantum efficiency η, is then given by the processes that directly result in radiative relaxation, $p_a p_r$, plus all $Yb^{3+}\rightarrow Yb^{3+}$ energy migration steps that ultimately result in a radiative relaxation, $p_a[(1-p_r)p_t]^k p_r$. Since $|(1-p_r)p_t|\leq 1$, we obtain

$$\eta=p_a p_r\sum_{k=0}^{\infty}[(1-p_r)p_t]^k=\frac{p_a p_r}{1-p_t(1-p_r)}. \tag{5}$$

We can now modify Eq. (1) to take into account these competing processes and find for the cooling efficiency in the presence of impurities

$$\eta_{cool}=\frac{\eta\bar{E}_F-E_P}{E_P}. \tag{6}$$

For the ideal case shown in Fig. 1(a) we have $p_a=p_r=p_t=1$ and obtain the ideal cooling efficiency of Eq. (1). In the presence of impurities all three probabilities may be <1. The resulting $\eta<1$ reduces the cooling efficiency via a decrease of the effective mean fluorescence energy.

In Sec. IV, we will study the relative contributions of various processes to overall heating. Processes that do not lead to a cooling event [Eq. (5)] must ultimately result in heating. The probability of a heating event therefore is $(1-\eta)$. As illustrated in Fig. 4, heating events occur either via background absorption with probability $(1-p_a)$ or via energy transfers from Yb^{3+} to impurities. The latter probability is thus given by $(1-\eta)-(1-p_a)$, i.e., $(p_a-\eta)$. The ratio γ of heating from Yb^{3+} energy-transfer processes to total heating can therefore be written as

$$\gamma=\frac{p_a-\eta}{1-\eta}. \tag{7}$$

In the following sections we will determine p_a, p_r, and p_t from spectroscopic and structural data to obtain a quantitative description of the cooling efficiency in the presence of transition-metal and OH impurities in ZBLAN:Yb^{3+}.

C. Structural model for ZBLAN glass

The calculation of rates for $Yb^{3+}\rightarrow Yb^{3+}$ energy migration and for energy transfer from Yb^{3+} to impurities [$w_{0i}^{(nr)}(T)$ in Eqs. (3) and (4)] requires knowledge of the spatial arrangement of the donor and acceptor ions involved in the transfers, i.e. the respective ion pair distribution function (PDF). The

PDF, $N_{M_1\text{-}M_2}(R)$, in disordered systems is generally defined as the cumulative number of M_1-M_2 atom pairs up to distance R from the central atom M_1 according to $N_{M_1\text{-}M_2}(R) = \int_{r=0}^{R} n_{M_1\text{-}M_2}(r)dr$, where $n_{M_1\text{-}M_2}(r)$ is the number of atom pairs in the distance interval dr at distance R from the central atom M_1. $n_{M_1\text{-}M_2}(r)$ has units of atoms per unit length and is the quantity relevant to a donor-to-acceptor energy transfer since it represents the number of available acceptor ions in a shell dr at r from a donor ion. We will use this quantity in conjunction with a model for electric-dipole-electric-dipole (ED) mediated energy transfer in Secs. III D and III E. The ED interactions introduce a characteristic r^{-6} distance dependence to the energy-transfer rate. The total energy-transfer rate from a central M_1 (donor) to all M_2 (acceptors) in the solid is therefore proportional to the radial integral

$$\Pi^{\mathrm{ED}}_{M_1\text{-}M_2} = \int_0^\infty \frac{n_{M_1\text{-}M_2}(r)}{r^6} dr. \tag{8}$$

While PDFs can be easily derived for crystals with a known structure, it is more difficult to obtain this information for a material with no long-range order such as ZBLAN glass. In the following, we will use molecular dynamics calculations to obtain the PDFs between La^{3+} and the main constituents of pure ZBLAN (Refs. 30 and 31) and between La^{3+} and divalent (M^{2+}) and trivalent (M^{3+}) transition-metal impurities doped into ZBLAN. The simulations are carried out at constant volume, assuming a cubic cell (d=30.08 Å) containing 1965 ions (265 Zr^{4+}, 100 Ba^{2+}, 20 La^{3+}, 15 Al^{3+}, 100 Na^{+}, 1465 F^{-}) representing the 53%ZrF_4-20%BaF_2-4%LaF_3-3%AlF_3-20%NaF (mol. %) ZBLAN glass composition with a density of 4.35 g/cm^3. The model uses a Born-Mayer type potential, $\Phi_{ij} = (e^2 Z_i Z_j / 4\pi\varepsilon_0 R_{ij}) + B_{ij} e^{-R_{ij}/\rho}$. The Coulombic interactions in the first term use formal ionic charges Z_i. The second term is the repulsive short-range interaction characterized by B_{ij} (Ref. 31) and the "softness parameter" ρ=0.3 Å that defines the radial shape of the ion wave functions.[32,33] The classical equations of motion were integrated by using Verlet's algorithm with a time step of 1 fs. After 2×10^4 time steps at 3000 K, the temperature of the simulation was lowered from 3000 K to 293 K for 5×10^4 time steps, and the system was annealed at 293 K for 2×10^4 time steps to reach the final equilibrium structure. The final simulated structure was obtained by averaging 20 such calculations with different sets of random initial coordinates. The simulations of ZBLAN containing a transition-metal impurity, M($3d$), replaced 5 of the 20 La^{3+} ions in the cubic cell with a generic divalent or trivalent M($3d$) ion. Simulations with effective ionic radii (r_{eff}) of M($3d$) ranging from 0.65 to 0.95 Å in steps of 0.05 Å were carried out. Transition-metal ions were found to prefer fluoride coordination numbers ranging from 5.6 to 6.4. This is in agreement with optical absorption studies that found a pronounced tendency for $3d$ ions towards a sixfold octahedral coordination in ZBLAN.[34–36] The one exception is Cu^{2+} in ZBLAN, which has a tetragonally distorted symmetry due to the Jahn-Teller effect.[35] This effect is not included in our model and is ignored in the following analysis. Specific transition-metal ions were then assigned to the calculations based on their published r_{eff} for sixfold fluoride coordination.[37]

The final averaged ZBLAN structures yield the PDFs from which the corresponding radial integrals $\Pi^{\mathrm{ED}}_{\mathrm{La\text{-}M}}$ can be calculated using Eq. (8). The radial-integral values are the main result of our molecular-dynamics simulations, and they are summarized in Table I. We assume the active ion Yb^{3+} to replace La^{3+} without inducing any structural change when doped into ZBLAN. The radial integrals and thus PDFs relevant to $Yb^{3+}\rightarrow Yb^{3+}$ energy migration and $Yb^{3+}\rightarrow M(3d)$ energy-transfer processes are those of La^{3+} with La^{3+} as well as with M($3d$). In Sec. III E and the Appendix, we will study the role of OH^{-} in ZBLAN:Yb^{3+} and use the PDFs of La^{3+} with Zr^{4+}, Ba^{2+}, La^{3+}, Al^{3+}, and Na^{+}.

The r^{-6} dependence of $\Pi^{\mathrm{ED}}_{\mathrm{La\text{-}M}}$ strongly suppresses long-range contributions, and the $\Pi^{\mathrm{ED}}_{\mathrm{La\text{-}M}}$ are primarily determined by the local glass structure. Therefore, the radial-integral values converge quite rapidly with increasing number of averaged structures. This is illustrated in Fig. 5 for each ion pair: from the radial-integral values calculated for each the 20 structures, all possible subsets with $n<20$ values were selected and their average plotted as a function of n. The total spread of the averages decreases rapidly as n increases. For n=20, the magnitude of the total spread is small compared to the average, indicating that averaging 20 structural calculations yields a sufficiently well converged $\Pi^{\mathrm{ED}}_{\mathrm{La\text{-}M}}$ value for all ion pairs in the context of this study.

D. Energy transfer

The $Yb^{3+}\rightarrow Yb^{3+}$ and $Yb^{3+}\rightarrow$Impurity energy transfers critically depend on the resonance between the donor (Yb^{3+}) ion emission line and the acceptor ion absorption line. On the atomic scale, the linewidths are governed by homogeneous broadening, which increases with temperature as $\sim T^2$. The probability for resonant energy transfer is proportional to the spectral overlap between the homogeneously broadened donor emission and acceptor absorption lines.[38] Energy transfer between corresponding crystal-field transitions on two identical ions in a perfect crystal is exactly resonant, i.e., the spectral overlap is unity and independent of temperature. In disordered systems such as Yb^{3+} doped glass, however, there is a distribution of local Yb^{3+} coordination geometries, which leads to a temperature-independent (static) inhomogeneous broadening of the crystal-field transitions. At the atomic level, an $Yb^{3+}\rightarrow Yb^{3+}$ energy transfer that is resonant in a perfect crystal will, on average, become increasingly nonresonant with increasing disorder and thus require the assistance of phonons. Furthermore, the line shape measured on such a bulk sample has contributions from inhomogeneous broadening and thus may not be representative of the atomic (i.e., homogeneous) properties. Using such inhomogeneously broadened line shapes to calculate the spectral overlap in the context of Dexter's theory of *resonant* energy transfer[38] ignores the presence of phonon-assisted processes. Doing so will lead to an overestimate of the energy-transfer probability since phonon-assisted processes are generally less efficient than purely resonant ones. For our study this implies that we may overestimate the effect of Yb^{3+} energy

TABLE I. Radial integrals $\Pi^{ED}_{La\text{-}M}$ [Eq. (8)] calculated from the r^{-6} weighted PDFs obtained from the molecular-dynamics simulations for ZBLAN glass with the standard composition given by the ion concentrations c. The $\Pi^{ED}_{La\text{-}M}$ values are characteristic for this particular ZBLAN composition. They have to be scaled by the respective Yb^{3+} and transition-metal ion concentrations for the calculation of $Yb^{3+} \rightarrow Yb^{3+}$ and $Yb^{3+} \rightarrow M(3d)$ energy-transfer rates. For the calculation of transition-metal doped ZBLAN, 1% of a transition metal was introduced at the expense of the La^{3+} concentration. The effective ionic radii (r_{eff}) of transition metals in sixfold fluoride coordination (Ref. 37), rounded to the next 0.05, were assumed as r_{eff}. Both Fe^{2+} and Co^{2+} are assumed to be in the high-spin (HS) configuration in the crystal-field potential of the fluoride coordination.

		Effective ionic radius r_{eff} [Å]		
Ion (M)	c [mol. %]	from Ref. 37 (sixfold fluoride coordination)	Assumed for present calculation	$\Pi^{ED}_{La\text{-}M}$ [10^{55} m^{-6}]
Zr^{4+}	53			132.2
Ba^{2+}	20			44.15
La^{3+}	4			8.408
Al^{3+}	3			8.967
Na^{+}	20			67.13
Cu^{2+}	1	0.87	0.85	3.596
Fe^{2+} (HS)	1	0.910	0.90	3.106
Co^{2+} (HS)	1	0.875	0.90	3.106
Ni^{2+}	1	0.840	0.85	3.596
V^{3+}	1	0.780	0.80	2.498
Ti^{3+}	1	0.81	0.80	2.498
Cr^{3+}	1	0.755	0.75	2.738

migration to impurities and thus overestimate the effect of impurities on the cooling efficiency. Therefore, the results of our study should be viewed as a worst case.

Let us look in more detail at the relative magnitude of homogeneous and inhomogeneous broadening in ZBLANP:Yb^{3+}. The crystal-field transition with the highest spectral overlap of absorption and emission, and therefore the most significant contribution to $Yb^{3+} \rightarrow Yb^{3+}$ energy transfer, is the transition between the lowest crystal-field levels of the $^2F_{7/2}$ ground-state and $^2F_{5/2}$ excited-state multiplets. These $^2F_{7/2}(0) \leftrightarrow {}^2F_{5/2}(0)$ transitions correspond to the dominant absorption and emission bands around 975 nm (see Fig. 2). Lei *et al.* have measured the $^2F_{7/2}(0) \leftrightarrow {}^2F_{5/2}(0)$ temperature-independent inhomogeneous ($\Delta\nu_{inhom}$) and temperature-dependent homogeneous ($\Delta\nu_{hom}$) linewidths in ZBLANP:Yb^{3+}.[27] Above ~370 K, $\Delta\nu_{hom}$ dominates $\Delta\nu_{inhom}$, and the $Yb^{3+} \rightarrow Yb^{3+}$ energy transfer is purely resonant. The energy transfer becomes increasingly nonresonant with decreasing temperature as $\Delta\nu_{hom}$ decreases. The resulting energy mismatch, δE, between two Yb^{3+} ions undergoing a $^2F_{7/2}(0) \leftrightarrow {}^2F_{5/2}(0)$ energy transfer is limited however to ~28 cm^{-1} (Ref. 27) by the inhomogeneous linewidth. For temperatures above ~40 K, $\Delta\nu_{inhom}$ and thus δE are smaller than the thermal energy kT. The phonon density-of-states is sufficiently high at these temperatures such that there are always phonon modes available to assist in either an endothermic ($\delta E < 0$) or an exothermic ($\delta E > 0$) $^2F_{7/2}(0) \leftrightarrow {}^2F_{5/2}(0)$ energy transfer.[39] In this regime, $Yb^{3+} \rightarrow Yb^{3+}$ energy migration is a sequence of endothermic and exothermic energy transfers within the inhomogeneously broadened $^2F_{7/2}(0) \leftrightarrow {}^2F_{5/2}(0)$ line. On average, this energy migration neither deposits nor extracts heat from the phonon system, and it will therefore have no effect on the cooling efficiency.

Given the above considerations, we will describe $Yb^{3+} \rightarrow Yb^{3+}$ and $Yb^{3+} \rightarrow$Impurity energy transfers in Dexter's framework of resonant energy transfer.[38] If present, electric-dipole (ED) interactions typically dominate all other interactions, such as higher-order multipole and exchange interactions, by orders of magnitude. We therefore restrict the model to ED-mediated energy transfer. The probability for such a transfer from a donor (d) to an acceptor (a) is given by[38]

$$P^{ED}_{da} = \frac{3\hbar^4 c^4 Q_a}{4\pi n^4 R^6 \tau_d}\left(\frac{\varepsilon}{\varepsilon_c\sqrt{\kappa}}\right)^4 \int \frac{F_d(E)F_a(E)}{E^4}dE = \frac{C^{ED}_{da}}{R^6}, \quad (9)$$

where τ_d is the donor (electric dipole) radiative lifetime, $Q_a = \int \sigma(E)dE$ is the acceptor (electric dipole) absorption line strength, R is the distance between donor and acceptor, n is the refractive index, and the local-field-correction term $(\varepsilon/\varepsilon_c\sqrt{\kappa}) \cong 1$. The line shape functions for donor emission, $F_d(E)$, and acceptor absorption, $F_a(E)$, are in units of inverse energy and normalized, i.e., $\int F(E)dE = 1$, such that the transition cross-section is given by $\sigma(E) = QF(E)$. The energy-transfer constant C^{ED}_{da} combines these factors and has units of m^6/s.

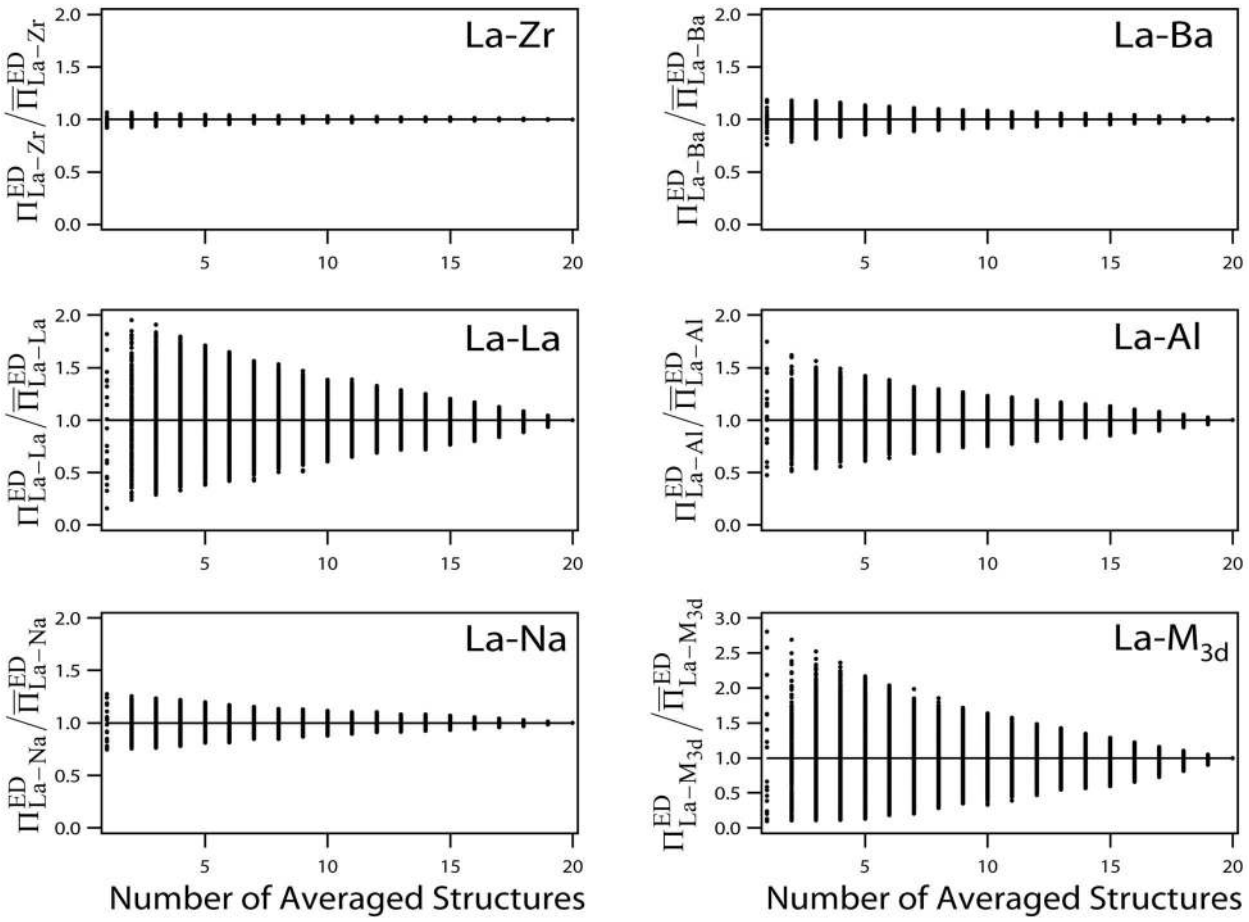

FIG. 5. Total spread of radial integral values, $\Pi^{ED}_{La\text{-}M}$ [Eq. (8)], as a function of the number of averaged molecular-dynamics structures, n. The radial-integral values are normalized to the respective value obtained from averaging $n=20$ molecular-dynamics structures, $\bar{\Pi}^{ED}_{La\text{-}M}$. The $n=20$ average yields a sufficiently well converged value for all ion pairs in the context of this study.

The total energy-transfer rate, $w^{ED}_{da}(T)$, from a donor to a spatial distribution of acceptor ions is then given by

$$w^{ED}_{da}(T) = c_a \Pi^{ED}_{da} C^{ED}_{da}(T), \tag{10}$$

where Π^{ED}_{da} is the radial integral for the *d-a* pair [Eq. (8)], $C^{ED}_{da}(T)$ is the ED-mediated energy-transfer constant at temperature T [Eq. (9)], and c_a is the acceptor concentration *relative* to that utilized for calculating Π^{ED}_{da}. Energy transfer rates calculated from Eq. (10) enter Eqs. (3) and (4) as nonradiative processes competing with Yb^{3+} radiative relaxation and Yb^{3+} energy migration, respectively.

The relevant energy-transfer constants $C^{ED}_{da}(T)$ are now derived from experimental data. The various factors that define $C^{ED}_{Yb\text{-}Yb}$ are available from absorption (Fig. 2, top), emission (Fig. 2, bottom), and lifetime (Table II) measurements of ZBLAN:Yb^{3+}. Table II summarizes the relevant quantities for $Yb^{3+} \rightarrow Yb^{3+}$ energy transfer. The experimental data base for transition metal ions, M(3*d*), in ZBLAN, and therefore $C^{ED}_{Yb\text{-}M(3d)}$, is less complete. France *et al.* report a comprehensive spectroscopic study of 3*d* transition metal ions in ZBLAN,[35] from which absorption line shapes as well as absolute absorption cross-sections can be derived for room temperature (see Fig. 6). Energy-transfer constants $C^{ED}_{Yb\text{-}M(3d)}$ calculated using this data are summarized in Table II. No comprehensive low-temperature data is available. The Cu^{2+}, Fe^{2+}, Co^{2+},Ni^{2+}, V^{3+}, Ti^{3+}, and Cr^{3+} absorption spectra (Fig. 6) are substantially broader than the Yb^{3+} emission spectrum (Fig. 2, bottom). Therefore, the spectral overlap integral relevant for a resonant $Yb^{3+} \rightarrow M(3d)$ energy transfer is expected to be fairly independent of temperature. We assume for the following analysis that the transition-metal room-temperature spectra shown in Fig. 6 and the $C^{ED}_{Yb\text{-}M(3d)}$ calculated from them (Table II) are representative for the 70–300 K temperature range.

E. Multiphonon relaxation

Multiphonon relaxation is expected to dominate the relaxation of excited 3*d* transition-metal ions in ZBLAN. The strong electron-phonon coupling of the 3*d* metal ion transitions considered here makes radiative relaxation highly unlikely, and we assume the quantum efficiency of these ions to be zero. In contrast, the $^2F_{5/2} \rightarrow {}^2F_{7/2}$ transition on Yb^{3+} is only weakly coupled to the vibrational system, and the multiphonon relaxation rate, w_{mp}, follows the well-known energy gap law

TABLE II. Spectral parameters and calculated resonant energy-transfer constants C_{da}^{ED} for a Yb^{3+} donor and various acceptor ions in ZBLAN. The donor (Yb^{3+}) lifetime τ_d, the integrated activator absorption line strength Q_a, and the spectral overlap integral S were derived from experimental data (Ref. 40). The resonant energy-transfer constants C_{da}^{ED} were calculated from Eq. (9) using a refractive index of 1.48 (Ref. 40).

Donor (d)	Acceptor (a)	T[K]	$\tau_d=1/w_r$ [ms]	Q_a [10^{-44} m^2 J]	S [10^{92} J^{-5}]	C_{da}^{ED} [10^{-50} m^6/s]
Yb^{3+}	Yb^{3+}	300	1.825	1.195	259	0.842
		250	1.832	1.304	258	0.912
		200	1.845	1.346	252	0.912
		150	1.869	1.343	250	0.892
		100	1.894	1.377	238	0.860
		50	1.942	1.471	223	0.840
		10	1.898	1.578	218	0.903
	Cu^{2+}	300	1.825	68.1	56.8	10.5
	Fe^{2+}	300	1.825	12.4	48.4	1.64
	Co^{2+}	300	1.825	7.30	47.8	0.950
	Ni^{2+}	300	1.825	6.16	35.0	0.586
	V^{3+}	300	1.825	31.0	5.70	0.480
	Ti^{3+}	300	1.825	18.5	1.76	0.0884
	Cr^{3+}	300	1.825	36.8	0.614	0.0615

$$w_{mp} = \beta e^{-\alpha m}, \tag{11}$$

where m is the number of phonons created in the relaxation process, and β and α are constants characteristic for the host material.[41] For ZBLAN, $\beta=7.28\times10^{12}$ s^{-1} and $\alpha=4.8$.[42] The highest-energy vibration, typically a localized optical mode, is the most likely acceptor in a multiphonon relaxation process since it minimizes m. With a highest-energy optical mode of $\hbar\omega_{max}\approx580$ cm^{-1} (Ref. 40) and a minimum $^2F_{5/2}\rightarrow{}^2F_{7/2}$ energy gap of $\Delta E\approx9770$ cm^{-1} in ZBLAN:Yb^{3+},[40] it follows that $m=16.8$ and thus $w_{mp}\approx0$ from Eq. (11). Therefore, multiphonon relaxation of the $^2F_{5/2}$ excited state via interaction with the optical modes of the ZBLAN host can be neglected relative to radiative relaxation (see Table II). If, however, the $^2F_{5/2}\rightarrow{}^2F_{7/2}$ transition can couple to a high-energy vibrational mode of an impurity, such as the 3440 cm^{-1} stretching frequency of an OH ion,[43] one has $m<3$ and multiphonon relaxation will dominate radiative decay by orders of magnitude. The OH ion is an example of a vibrational impurity that effectively creates a "dark" Yb^{3+} ion.

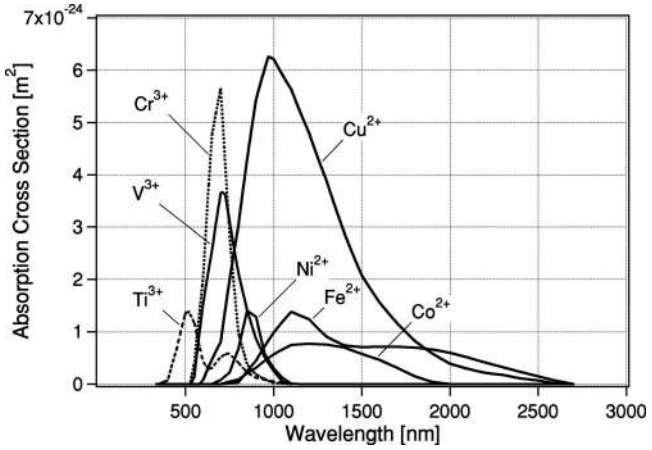

FIG. 6. Absorption cross-sections for various transition-metal ions in ZBLAN glass at room temperature; adapted from France *et al.* (Ref. 35).

The "classical" description of multiphonon relaxation in Eq. (11), and its various extensions proposed in the past, is insufficient for gaining an understanding of multiphonon relaxation in the presence of vibrational impurities in a solid. The multiphonon relaxation rate w_{mp} in Eq. (11) is an *integrated* rate, i.e., it contains the electron-phonon coupling with all oscillators of the host material (characterized by β and α). Thus, it can describe the absence of $^2F_{5/2}\rightarrow{}^2F_{7/2}$ multiphonon relaxation in pure ZBLAN:Yb^{3+} and illustrate the dominance of multiphonon relaxation if the host was comprised solely of high-energy vibrational modes. The energy-gap law in the form of Eq. (11) however provides no insight for the intermediate case of a low-energy phonon host material (such as ZBLAN) containing a small number of vibrational impurities (such as OH). In this case there are two types of Yb^{3+} ions: those Yb^{3+} that have a vibrational impurity in the first coordination shell and those Yb^{3+} that have no vibrational impurity in the first coordination shell. Let us define $w_v^{(1)}$ and $w_v^{(\infty)}$ as the multiphonon relaxation rates due to interactions with a vibrational impurity *within* the first coordination shell and interactions with a vibrational impurity *outside* the first coordination shell of Yb^{3+}, respectively. A high multiphonon relaxation rate is expected in the former case, but even in the latter case the Yb^{3+} ion can undergo multiphonon relaxation via interactions with vibrational impurities "nearby." The structural information from the molecular-dynamics simulations (Sec. III C) allows us to quantify $w_v^{(1)}$ and $w_v^{(\infty)}$ and to obtain a more detailed description of multiphonon relaxation in the presence of a vibrational impurity.

TABLE III. Estimated highest-energy local mode frequencies $\hbar\omega_{\text{M-F}}$ and multiphonon relaxation rate enhancement factors $\kappa_{\text{M-F}}$ [Eq. (A2)] for the standard composition of ZBLAN. On average, each metal ion contributes $Z_{\text{M}}\times c$ oscillators, where Z_{M} is the ion charge and c is the ion concentration. The frequencies $\hbar\omega_{\text{M-F}}$ were weighted with their relative contribution and adjusted to yield the observed $\hbar\omega_{\max}\approx 580\ \text{cm}^{-1}$ (Ref. 40) in the harmonic oscillator approximation.

Oscillator M-F	c [mol. %]	Z_{M}	Contribution [%]	Reduced Mass [u]	$\hbar\omega_{\text{M-F}}$ [cm^{-1}]	$\kappa_{\text{M-F}}$
Zr-F	53	4	72.35	15.72	571	1.031
Ba-F	20	2	13.65	16.69	554	1.001
La-F	4	3	4.10	16.71	554	$\equiv 1$
Al-F	3	3	3.07	11.15	678	1.251
Na-F	20	1	6.83	10.40	702	1.307
Bulk	100		100		580	

The detailed calculation outlined in the Appendix shows that only ~35% of the total multiphonon relaxation rate in *pure* ZBLAN glass is due to multiphonon relaxation in the first coordination shell. While most Yb^{3+} ions will not be affected *directly* by the addition of a small amount of an OH impurity, the sizeable magnitude of interactions of Yb^{3+} with vibrational modes *outside* the first coordination shell combined with the high vibrational energy of OH will substantially reduce the Yb^{3+} quantum efficiency.

The presence of a vibrational impurity will enhance the multiphonon relaxation constant, C^{1}_{mp} [Eq. (A4)], due to the higher vibrational energy and thus lower the number of phonons involved in the multiphonon relaxation compared to the pure ZBLAN glass. Assuming α and β to remain constant, the enhancement factor for $C^{(1)}_{mp}$ is $\exp[\alpha(m_{\text{host}}-m_v)]$, where m_{host} and m_v is the electronic energy gap bridged by the multiphonon relaxation expressed in quanta of the highest-energy mode of the host material ($\hbar\omega_{\max}$) and the vibrational impurity, respectively. In analogy to Eq. (10), we can express $w^{(\infty)}_v$ as

$$w^{(\infty)}_v = c_v C^{(1)}_{mp} e^{\alpha(m_{\text{host}}-m_v)} \sum_{\text{M}} Z_{\text{M}}\kappa_{\text{MF}}\Pi^{\text{ED}}_{\text{La-M}} \tag{12}$$

and $w^{(1)}_v$ as

$$w^{(1)}_v = c_v \frac{Z_{\text{La}} C^{(1)}_{mp} e^{\alpha(m_{\text{host}}-m_v)}}{R^{6}_{(1)}}, \tag{13}$$

where c_v is the concentration of the vibrational impurity relative to the total metal-ion concentration in ZBLAN:Yb^{3+}, Z_{M} is the ionic charge of ion M, κ_{MF} is the multiphonon relaxation rate enhancement factor [Eq. (A2) and Table III], and $R_{(1)}$ is the characteristic distance for multiphonon relaxation in the first coordination shell, assumed here as the average La-F distance in ZBLAN of 3.0 Å. The temperature dependence of the multiphonon relaxation rate in Eqs. (12) and (13) is given by $w_v(T)=w_v(T=0)/(1-e^{-\hbar\omega/kT})^m$.[44,45] The total multiphonon relaxation rate is then given by

$$w_v(T) = w^{(1)}_v(T) + w^{(\infty)}_v(T). \tag{14}$$

This is the rate that enters Eqs. (3) and (4) as one of the nonradiative processes competing with Yb^{3+} radiative relaxation and Yb^{3+} energy migration, respectively.

The effect of a small amount of vibrational impurities in ZBLAN:1 % Yb^{3+} on the cooling efficiency can be illustrated as follows. In impurity-free ZBLAN:Yb^{3+}, multiphonon relaxation is absent [Eq. (11)], and the Yb^{3+} ($^2F_{5/2}\rightarrow{}^2F_{7/2}$) quantum efficiency, $w_r/(w_r+w_{mp})$, is ~1.0. We now add 10 ppm of an OH impurity. With $m_{\text{host}}=9770\ \text{cm}^{-1}/580\ \text{cm}^{-1}=16.8$ and $m_v=9770\ \text{cm}^{-1}/3440\ \text{cm}^{-1}=2.84$, we find that $w^{(1)}_v=3.0\times10^6\ \text{s}^{-1}$ [Eq. (13)] and $w^{(\infty)}_v=57.2\ \text{s}^{-1}$ [Eq. (12)]. Clearly, the multiphonon relaxation rate of a Yb^{3+} ion with an OH impurity in its first coordination shell, $w^{(1)}_v$, is very high relative to the 300 K radiative relaxation rate of $w_r=548\ \text{s}^{-1}$ (Table II) and therefore reduces the quantum efficiency of this Yb^{3+} ion to <0.02%, creating a "dark" Yb^{3+}. But even for the vast majority of Yb^{3+} ions *without* an OH impurity in the *first* coordination shell, the quantum efficiency will be reduced substantially to $548\ \text{s}^{-1}/(548\ \text{s}^{-1}+57.2\ \text{s}^{-1})=0.905$, on average, by the presence of OH impurities nearby. This reduction is significant in the context of laser cooling.

The model for multiphonon relaxation described here is a substantial enhancement of the "classical" energy gap law [Eq. (11)]. It provides quantitative insight into multiphonon relaxation in the presence of vibrational impurities by using structural information via the radial integral $\Pi^{\text{ED}}_{\text{La-M}}$ derived from the molecular-dynamics calculations.

IV. DISCUSSION

There are a great number of impurities that have the potential to reduce the cooling efficiency in a rare-earth-doped solid. Impurities are present in the starting materials and can also be introduced during the synthesis of the cooler material. They include the range of transition metals, rare earths, complex ions, and molecular species, with $3d$ transition metals and H_2O/OH being the most ubiquitous impurities in commercially available starting materials. Of the rare-earth ions, Er^{3+} and Tm^{3+} are not only the most common impurities in Yb^{3+} starting materials but also the most efficient acceptors in nonradiative energy transfers from Yb^{3+}. Goldner *et al.* have shown that Er^{3+} and Tm^{3+} impurities in ZBLAN:Yb^{3+} degrade the cooling efficiency only at concen-

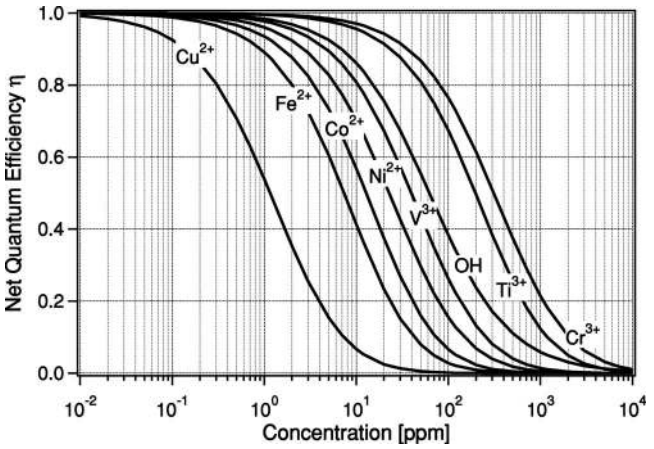

FIG. 7. Calculated net quantum efficiency η in ZBLAN:1 % Yb^{3+} as a function of impurity concentration at 120 K. The quenching curves were calculated from Eq. (5) and the data presented in Secs. III A to III E.

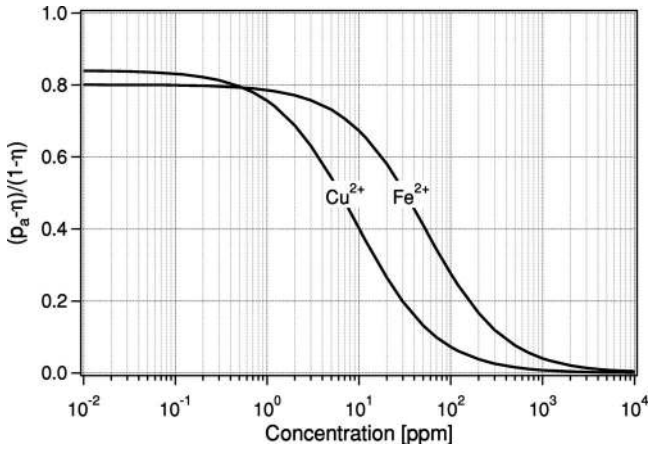

FIG. 8. Relative contribution of heating via energy transfer processes from Yb^{3+} [process "II" in Fig. 1(b)] to overall heating, $(p_a-\eta)/(1-\eta)$, for Cu^{2+} and Fe^{2+} in ZBLAN:1 % Yb^{3+} at 120 K calculated from Eq. (7) and the data presented in Secs. III A to III E.

trations of ~5 and ~500 ppm, respectively, and above and have a negligible effect on the cooling efficiency at trace concentrations.[26] We therefore exclude rare-earth impurities for the following analysis.

As evident from the preceding sections, detailed spectroscopic information is needed to quantitatively evaluate an impurity for its potential to degrade the cooling efficiency. The situation for ZBLAN glass is fortunate since there is a large body of work from the past two decades of developing this class of materials for passive and active fiber-optic applications. The quantitative absorption data available for Cu^{2+}, Fe^{2+}, Co^{2+}, Ni^{2+}, V^{3+}, Ti^{3+}, and Cr^{3+} in ZBLAN,[35] while being a subset of potentially detrimental transition-metal impurities, is representative of metal impurities commonly present in commercial materials. We thus have a data base for ZBLAN that enables the study of trends in support of developing a synthesis strategy for next-generation high-performance ZBLAN:Yb^{3+} glass.

Transition metal ion impurities degrade the net Yb^{3+} quantum efficiency η [Eq. (5)] and thus the cooling efficiency η_{cool} [Eq. (6)] by (i) becoming acceptors in energy transfer processes from Yb^{3+} and (ii) contributing to background absorption, both followed by multiphonon relaxation [Fig. 1(b)]. Both of these processes become increasingly active with increasing absorption cross section and spectral overlap with the Yb^{3+} transitions in the ~1 μm wavelength range. The OH vibrational impurity decreases the cooling efficiency by directly quenching the Yb^{3+} $^2F_{5/2}$ excited state [Fig. 1(b)]. The net Yb^{3+} quantum efficiency, η, as a function of impurity concentration in ZBLAN:1 % Yb^{3+} is shown in Fig. 7 for 120 K. These quenching curves were calculated from Eq. (5) and the data presented in Secs. III A to III E. The quenching curves are only very slightly temperature dependent in the context of our model. The impact of the various impurities on η ranges over more than two orders of magnitude. Specifically, the impurity concentrations at the inflection points of the quenching curves are approximately inversely proportional to the product $Q_a \times S \times \Pi_{da}^{ED}$, indicating that energy-transfer processes from Yb^{3+} [process "II" in Fig. 1(b)] primarily drive the reduction in quantum efficiency, rather than background absorption [process "III" in Fig. 1(b)]. The contribution of heating from Yb^{3+} energy transfer processes to total heating is given by $(p_a-\eta)/(1-\eta)$ [Eq. (7)]. This quantity is plotted in Fig. 8 for the two impurities Cu^{2+} and Fe^{2+} in ZBLAN:1 % Yb^{3+}. Quenching by energy-transfer processes from Yb^{3+} is dominant at low impurity concentrations. As the impurity concentration increases, the quantum efficiency η is already reduced to <90% (see Fig. 7) before quenching by background absorption becomes dominant.

We have seen in Eq. (6) that the cooling efficiency η_{cool} is sensitive to the net quantum efficiency η. This is particularly pronounced for a system like Yb^{3+} that has a small energy difference $\bar{E}_F$-E_P relative to the pump energy E_P. A small reduction of η from 1 is therefore sufficient to dramatically reduce η_{cool}. This is further exacerbated as the temperature, and thus $\bar{E}_F$-E_P, decreases (see Fig. 3). As a result, η_{cool} is highly sensitive to the presence of impurities (Fig. 7). This is shown in Fig. 9, which plots η_{cool} [Eq. (6)] as a function of impurity concentrations at 120 K and 208 K, a desired cryogenic temperature and the current record-cooling temperature, respectively. The common Cu^{2+}, Fe^{2+}, Co^{2+}, and Ni^{2+} metal ions are the most problematic, as expected from their near-infrared absorption that overlaps well with the Yb^{3+} emission spectrum and has a large cross section (Fig. 6). Likewise, OH has a pronounced impact on the cooling efficiency.

We can now establish upper impurity concentration limits for laser cooling in ZBLAN:Yb^{3+} at different operating temperatures. Figure 10 is the main result of our calculation. It shows threshold impurity concentrations at which the cooling efficiency η_{cool} reaches 90% of the theoretically possible value shown in Fig. 3. Clearly, laser cooling to cryogenic temperatures with ZBLAN:1 % Yb^{3+} requires ultrapure materials with 3d transition metal and OH concentrations well below 1 ppm. Several types of impurities will be present simultaneously in an actual material, which further decreases

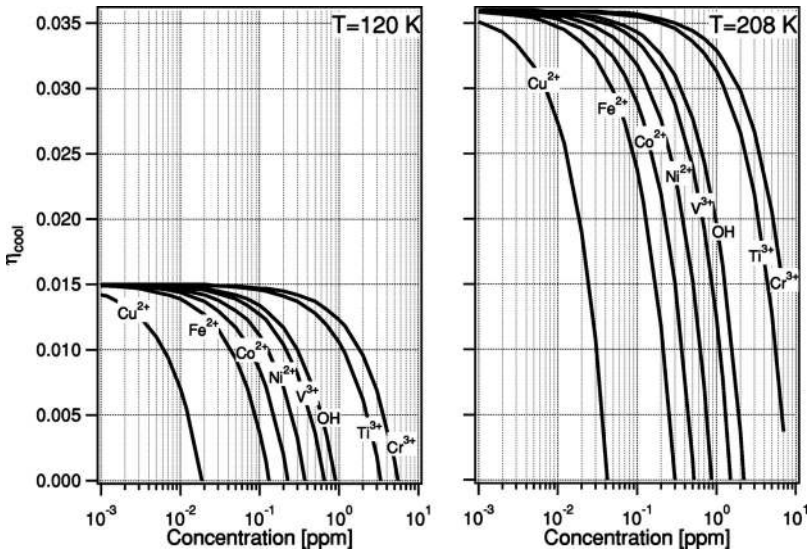

FIG. 9. Calculated [Eq. (6)] cooling efficiency, η_{cool}, for ZBLAN:1 % Yb^{3+} as a function of impurity concentration at 120 K (left) and 208 K (right).

these *individual* threshold concentrations since the impact of the different impurities on η_{cool} is cumulative. The current ZBLAN:Yb^{3+} laser-cooling record achieved 208 K with a net cooling efficiency of ~0.003.[7] From Fig. 9 we conclude that this must have been a sample with divalent transition-metal impurities well below 1 ppm and trivalent transition-metal and OH impurities in the low ppm range. A further 20–30 fold reduction in impurity concentrations is required to achieve efficient laser cooling at the application-relevant temperature of 120 K. In that case, none of the divalent and OH impurities must exceed 100 ppb, and the Cu^{2+} impurity must be essentially eliminated (<2 ppb).

In Sec. III D we have concluded that the $Yb^{3+} \rightarrow Yb^{3+}$ energy-transfer rate calculated from the model of resonant energy transfer [Eq. (9)] represents an upper limit. The model may therefore overestimate the transport of energy via Yb^{3+} ions to impurities, and thus overestimate the *absolute* value of impurity concentrations in Figs. 7–10. However, our conclusions on the *relative* importance of the various impurities as well as on the required purity improvement are not affected by this uncertainty and remain valid.

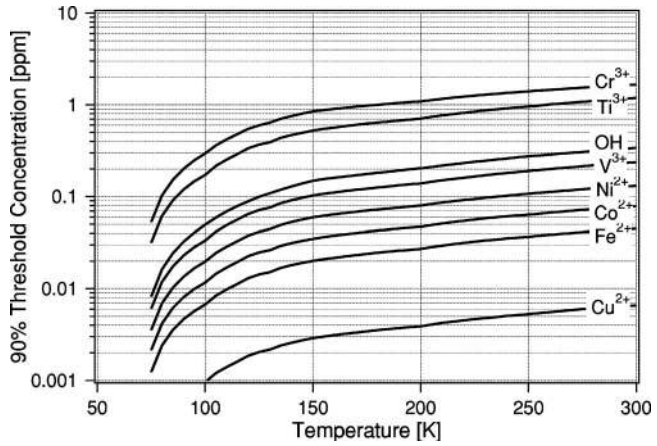

FIG. 10. Calculated impurity threshold concentrations for which the cooling efficiency, η_{cool}, reaches 90% of the ideal value (see Fig. 3) in ZBLAN:1 % Yb^{3+}.

V. CONCLUSIONS

We have developed a detailed model for optical refrigeration in ZBLAN:Yb^{3+} in the presence of impurities. The existing extensive spectroscopic data on ZBLAN:Yb^{3+} in combination with a molecular-dynamics calculation of ZBLAN has enabled us to quantify the competition of radiative processes with a variety of nonradiative processes and to calculate cooling efficiencies in the presence of different types of 3*d* transition-metal ions as well as OH. Laser cooling in ZBLAN:Yb^{3+} is highly sensitive to the presence of these impurities, which are found to act primarily as acceptors and quenching sites in energy-transfer processes from Yb^{3+}. Divalent 3*d* transition-metal ions are particularly problematic due to their strong near-infrared absorptions with good spectral overlap with the Yb^{3+} emission. Specifically, efficient laser cooling at a desired cryogenic temperature of 120 K is only possible if the concentration of such impurities is reduced to <100 ppb. In our estimate, this represents a 20–30 fold improvement in purity over the current record-holding ZBLAN:1 % Yb^{3+} sample. Advanced purification techniques targeted at specifically reducing the most problematic Cu^{2+}, Fe^{2+},Co^{2+}, Ni^{2+}, and OH impurities will be required to create a material that will be able to offer adequate cooling at application-relevant temperatures.

APPENDIX: MULTIPHONON RELAXATION

Let us define $w_{\mathrm{host}}^{(1)}$ and $w_{\mathrm{host}}^{(\infty)}$ as the multiphonon relaxation rates due to interactions with local modes *within* the first coordination shell and interactions with local modes *outside* the first coordination shell of Yb^{3+} in *pure* ZBLAN, respectively. Using Eq. (11), the total multiphonon relaxation rate can then be written as

$$w_{mp} = \beta e^{-\alpha m} = w_{\mathrm{host}}^{(1)} + w_{\mathrm{host}}^{(\infty)}. \tag{A1}$$

Let us assume that the observed highest-energy optical mode $\hbar\omega_{\max} \approx 580\ \mathrm{cm}^{-1}$ in ZBLAN (Ref. 40) is the concentration-weighted average of all local M-F stretching modes, where M=Zr, Ba, La, Al, Na. Let us further assume that the M-F

frequency $\hbar\omega_{\text{M-F}}$ simply scales with the square root of the reduced mass (harmonic oscillator) $\mu=m_{\text{M}}m_{\text{F}}/(m_{\text{M}}+m_{\text{F}})$. The $\hbar\omega_{\text{M-F}}$ calculated from this model are summarized in Table III. Compared to La^{3+}, all other metal ions are lighter and corresponding M-F frequencies are higher and therefore have an exponentially higher contribution to the multiphonon relaxation rate on the rare-earth site by the factor

$$\kappa_{\text{M-F}} = \exp\left(\frac{\hbar\omega_{\text{M-F}}}{\hbar\omega_{\text{La-F}}} - 1\right). \tag{A2}$$

Assuming that multiphonon relaxation is mediated by electric-dipole (ED) interactions, the two contributions $w_{\text{host}}^{(1)}$ and $w_{\text{host}}^{(\infty)}$ to w_{mp} can now be evaluated, in analogy to Eq. (10), according to

$$w_{mp} = w_{\text{host}}^{(1)} + w_{\text{host}}^{(\infty)} = \frac{Z_{\text{La}}C_{mp}^{(1)}}{R_{(1)}^6} + C_{mp}^{(1)}\sum_{\text{M}} Z_{\text{M}}\kappa_{\text{M-F}}\Pi_{\text{La-M}}^{\text{ED}}, \tag{A3}$$

where $C_{mp}^{(1)}$ is the multiphonon relaxation constant for the first coordination shell, Z_{M} is the ionic charge of ion M, $\Pi_{\text{La-M}}^{\text{ED}}$ is the radial integral [Eq. (8)], and $R_{(1)}$ is the characteristic distance for multiphonon relaxation in the first coordination shell, assumed here as the average La-F distance in ZBLAN of 3.0 Å. On average, each metal ion contributes Z_{M} oscillators for a coordination with singly negatively charged ions. We therefore carry out the summation in Eq. (A3) over all metal ions M weighted by the respective Z_{M}. By combining Eqs. (A1) and (A3), the multiphonon relaxation constant for the first coordination shell becomes

$$C_{mp}^{(1)} = \frac{R_{(1)}^6\beta e^{-\alpha m}}{Z_{\text{La}} + R_{(1)}^6\sum_{\text{M}} Z_{\text{M}}\kappa_{\text{M-F}}\Pi_{\text{La-M}}^{\text{ED}}} \tag{A4}$$

and evaluates to $C_{mp}^{(1)}=5.8\times10^{-81}$ m^6 s^{-1} with the parameters given in Sec. III E and Tables I–III. As a result we find that $w_{\text{host}}^{(1)}/w_{mp}=0.345$, i.e. only 34.5% of the total multiphonon relaxation rate in pure ZBLAN glass is due to multiphonon relaxation in the first coordination shell.

[1] R. I. Epstein, M. I. Buchwald, B. C. Edwards, T. R. Gosnell, and C. E. Mungan, Nature (London) **377**, 500 (1995).
[2] C. E. Mungan, M. I. Buchwald, B. C. Edwards, R. I. Epstein, and T. R. Gosnell, Phys. Rev. Lett. **78**, 1030 (1997).
[3] C. E. Mungan, M. I. Buchwald, B. C. Edwards, R. I. Epstein, and T. R. Gosnell, Appl. Phys. Lett. **71**, 1458 (1997).
[4] X. Luo, M. D. Eisaman, and T. R. Gosnell, Opt. Lett. **23**, 639 (1998).
[5] M. T. Murtagh, G. H. Sigel, J. C. Fajardo, B. C. Edwards, and R. I. Epstein, J. Non-Cryst. Solids **253**, 50 (1999).
[6] T. R. Gosnell, Opt. Lett. **24**, 1041 (1999).
[7] J. Thiede, J. Distel, S. R. Greenfield, and R. I. Epstein, Appl. Phys. Lett. **86**, 154107 (2005).
[8] A. Rayner, M. E. J. Friese, A. G. Truscott, N. R. Heckenberg, and H. Rubinsztein-Dunlop, J. Mod. Opt. **48**, 103 (2001).
[9] B. Heeg, M. D. Stone, A. Khizhnyak, G. Rumbles, G. Mills, and P. A. DeBarber, Phys. Rev. A **70**, 021401(R) (2004).
[10] J. Fernandez, A. Mendioroz, A. J. Garcia, R. Balda, and J. L. Adam, Phys. Rev. B **62**, 3213 (2000).
[11] J. Fernandez, A. Mendioroz, R. Balda, M. Voda, M. Al-Saleh, A. J. Garcia-Adeva, J. L. Adam, and J. Lucas, Proc. SPIE **4645**, 135 (2002).
[12] S. R. Bowman and C. E. Mungan, Appl. Phys. B **B71**, 807 (2000).
[13] C. E. Mungan, S. R. Bowman, and T. R. Gosnell, Intl. Conf. on Lasers, 4-8 Dec. 2000, Albuquerque, NM, USA.
[14] R. I. Epstein, J. J. Brown, B. C. Edwards, and A. Gibbs, J. Appl. Phys. **90**, 4815 (2001).
[15] A. Mendioroz, J. Fernandez, M. Voda, M. Al-Saleh, R. Balda, and A. J. Garcia-Adeva, Opt. Lett. **27**, 1525 (2002).
[16] S. Bigotta, D. Parisi, L. Bonelli, A. Toncelli, M. Tonelli, and A. Di Lieto, J. Appl. Phys. **100**, 013109 (2006).
[17] S. Bigotta, D. Parisi, L. Bonelli, A. Toncelli, A. Di Lieto, and M. Tonelli, Opt. Mater. **28**, 1321 (2006).
[18] C. W. Hoyt, M. Sheik-Bahae, R. I. Epstein, B. C. Edwards, and J. E. Anderson, Phys. Rev. Lett. **85**, 3600 (2000).
[19] C. W. Hoyt, M. P. Hasselbeck, M. Sheik-Bahae, R. I. Epstein, S. Greenfield, J. Thiede, J. Distel, and J. Valencia, J. Opt. Soc. Am. B **20**, 1066 (2003).
[20] C. W. Hoyt, W. Patterson, M. P. Hasselbeck, M. Sheik-Bahae, R. I. Epstein, J. Thiede, and D. Seletskiy, Quantum Electronics and Laser Science (QELS). Postconference Digest, 1-6 June 2003, Baltimore, MD, USA.
[21] W. Patterson, M. P. Hasselbeck, M. Sheik-Bahae, S. Bigotta, D. Parisi, A. Toncelli, M. Tonelli, R. I. Epstein, and J. Thiede, Lasers and Electro-Optics (CLEO), 16-21 May 2004, San Francisco, CA, USA.
[22] J. Fernandez, A. J. Garcia-Adeva, and R. Balda, Phys. Rev. Lett. **97**, 033001 (2006).
[23] M. G. Drexhage, in *Treatise on Materials Science and Technology*, edited by M. Tomozawa and R. H. Doremus (Academic, New York, 1985), Vol. 26, p. 151.
[24] *Fluoride Glasses*, edited by A. E. Comyns, Critical Reports on Appl. Chem., Vol. 27 (John Wiley, New York, 1989).
[25] A. Rayner, N. R. Heckenberg, and H. Rubinsztein-Dunlop, J. Opt. Soc. Am. B **20**, 1037 (2003).
[26] P. Goldner and M. Mortier, J. Non-Cryst. Solids **284**, 249 (2001).
[27] G. Lei, J. E. Anderson, M. I. Buchwald, B. C. Edwards, and R. I. Epstein, Phys. Rev. B **57**, 7673 (1998).
[28] B. C. Edwards, M. I. Buchwald, and R. I. Epstein, Rev. Sci. Instrum. **69**, 2050 (1998).
[29] G. Lamouche, P. Lavallard, R. Suris, and R. Grousson, J. Appl. Phys. **84**, 509 (1998).
[30] H. Inoue, K. Soga, and A. Makishima, J. Non-Cryst. Solids **306**,

17 (2002).
[31] H. Ionue, K. Soga, and A. Makishima, J. Non-Cryst. Solids **298**, 270 (2002).
[32] F. G. Fumi and M. P. Tosi, J. Phys. Chem. Solids **25**, 31 (1964).
[33] M. P. Tosi and F. G. Fumi, J. Phys. Chem. Solids **25**, 45 (1964).
[34] Y. Ohishi, S. Mitachi, T. Kanamori, and T. Manabe, Phys. Chem. Glasses **24**, 135 (1983).
[35] P. W. France, S. F. Carter, and J. M. Parker, Phys. Chem. Glasses **27**, 32 (1986).
[36] C. K. Jorgensen and R. Reisfeld, Mater. Sci. Forum **19**, 593 (1987).
[37] R. D. Shannon and C. T. Prewitt, Acta Crystallogr. **B25**, 925 (1969).
[38] D. L. Dexter, J. Chem. Phys. **21**, 836 (1953).
[39] T. F. Soules and C. B. Duke, Phys. Rev. B **3**, 262 (1971).
[40] G. Lei, J. E. Anderson, M. I. Buchwald, B. C. Edwards, R. I. Epstein, M. T. Murtagh, and G. H. Sigel, IEEE J. Quantum Electron. **34**, 1839 (1998).
[41] L. A. Riseberg and H. W. Moos, Phys. Rev. **174**, 429 (1968).
[42] F. Auzel and F. Pelle, Proc. SPIE **3416**, 74 (1998).
[43] P. C. Schultz, L. J. B. Vacha, C. T. Moynihan, B. B. Harbison, K. Cadien, and R. Mossadegh, Mater. Res. Soc. Symp. Proc. **19**, 343 (1987).
[44] T. Miyakawa and D. L. Dexter, Phys. Rev. B **1**, 2961 (1970).
[45] R. Orbach, in *Optical Properties of Ions in Solids*, edited by B. Di Bartolo (Plenum Press, New York, 1975), p. 355.